Multiphoton photoemission and electric-field-induced optical second-harmonic generation as probes of charge transfer across the Si/SiO_2 interface

J. G. Mihaychuk,* N. Shamir,† and H. M. van Driel‡
Department of Physics, University of Toronto, Toronto, Canada M5S 1A7
(Received 26 May 1998)

Multiphoton photoemission (MPPE) and electric field-induced second-harmonic generation (EFISH) are used as complementary *in situ* probes of light-induced electron transfer across the $Si(100)/SiO_2$ interface. Pulses of ~ 150 fs duration with photon energy $1.55\ \text{eV} < \hbar\omega < 1.75$ eV at repetition rates of 250 kHz or 76 MHz impinge on samples with 1.6-nm-thick thermally grown oxides. Oxygen-assisted charging of the surface via internal photoemission from Si to SiO_2 is shown to increase (decrease) the EFISH intensity (MPPE current) with EFISH (MPPE) being sensitive to charge transfer at O_2 pressures $1 < P(O_2) < 10^3$ Torr $[10^{-5} < P(O_2) < 1$ Torr]. At 10^3 Torr and average (peak) irradiances 1 kW cm^{-2} (25 GW cm^{-2}), the surface charge density reaches 10^{13} cm^{-2}. Adsorption is shown to follow a Fowler-Guggenheim isotherm consistent with repulsion of charged species; an effective diffusion constant $D \sim 10^{-7}$ cm^2/s is obtained. The small residual EFISH/MPPE signal on return to vacuum conditions indicates transfer of some electrons to SiO_2 traps. [S0163-1829(99)07903-5]

I. INTRODUCTION

The properties of the Si/SiO_2 system form the basis of much of the semiconductor industry and are therefore the subject of intensive research. As metal-oxide-semiconductor (MOS) device dimensions penetrate further into the submicron regime, the properties of ultrathin (5 nm or less) oxides[1,2] on Si become more critical. Charge accumulation in SiO_2 is an important effect which can cause long-term drift in MOS devices. This can occur via trapping by defects,[3] but impinging or adsorbed gases can also assist film charging.[4]

Oxide charge is typically measured by capacitance-voltage and current-voltage methods.[3,5] However, optical second-harmonic generation (SHG) is a proven noninvasive, non-contact tool for studies of electronic and structural properties of Si/SiO_2,[6–17], MOS,[18–21] and metal-silicon[22–24] systems. Optical techniques offer the advantage of *in situ* measurements in the presence of gases or fluids and can also probe buried interfaces such as Si/SiO_2. It has been demonstrated that high repetition rate femtosecond laser pulses can yield high signal-to-noise ratios while minimizing sample heating effects.[10] In recent works, we have shown that electric field induced SHG (EFISH) is a sensitive probe of electron transfer in the Si/SiO_2 system.[6–8] When wafers exposed to O_2 gas are illuminated by 800-nm, 150-fs pulse trains,[7,8] the surface is efficiently charged via internal photoemission (IPE) of electrons from Si to SiO_2. Other gases have considerably reduced effects (a general mechanism of gas-induced surface charging will be proposed elsewhere[25]). From the intensity dependence of the charging time we showed[7] that IPE involves excitation of electrons from the Si valence band (VB) to the oxide conduction band (CB) by absorption of at least three photons. The relevant energy level scheme[26–29] is shown in Fig. 1. In addition to the band edges in Si/SiO_2, Fig. 1 shows the ground states of O_2 and of O_2^-, which likely forms following charging of the surface. Electron transfer to the surface decreases with increasing oxide thickness[7] and vanishes for oxides thicker than 10 nm. The resulting surface charge and superoxide ions[30,31] (O_2^-) strongly affect the electric field in Si near the Si/SiO_2 interface. Small irreversible changes in the EFISH response following evacuation of O_2 suggest transfer of charge from adsorbed O_2 to oxide traps. Since IPE alters the charge distribution, the laser acts as both pump and probe. Nevertheless, the IPE/EFISH combination opens up new opportunities for quantitatively studying surface charging effects for O_2 pressures $\geqslant 1$ mTorr and surface charge density $> 10^{11}$ cm^{-2}.

In this paper, using a $Si(100)/1.6$-nm SiO_2 wafer we offer results from multiphoton photoemission (MPPE) experiments to independently corroborate our EFISH studies and to demonstrate increased sensitivity to surface and bulk oxide charging effects. We also extend earlier EFISH work to in-

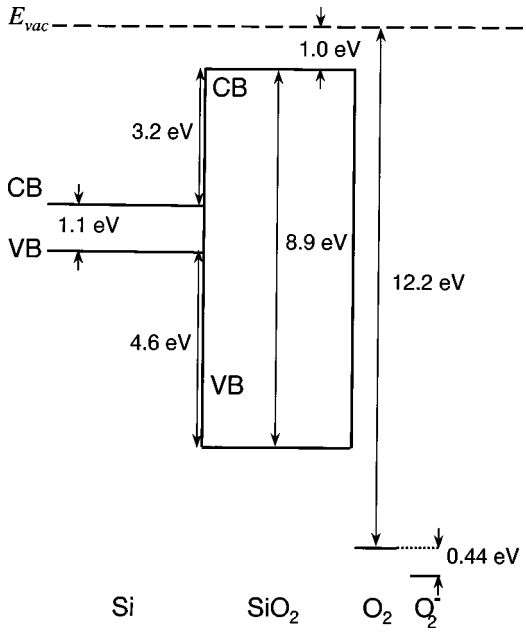

FIG. 1. Band-edge energies in Si/SiO_2: CB, conduction band; VB, valence band; E_{vac}, vacuum energy level. The ionization energy and electron affinity of O_2 are also shown.

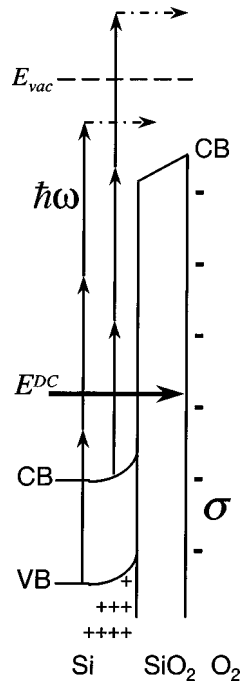

FIG. 2. Influence of IPE and charging of adsorbed O_2 on EFISH and MPPE: E^{dc}, static electric field in Si (solid horizontal arrow); $\hbar\omega$, photon energy; E_{vac}, vacuum energy level; CB, conduction band; VB, valence band; σ, surface charge density. Here three-photon absorption (vertical arrows) excites an electron (dot-dashed arrow) from the Si VB to the SiO_2 CB.

clude spectroscopic studies, and present a fundamental model of the EFISH time dependence under surface charging conditions. MPPE has previously been used to study[32–35] Si and[36,37] α-SiO_2, and both MPPE (Ref. 38) and EFISH (Refs. 22–24) have been applied separately to high-speed electro-optic sampling. However, EFISH and MPPE have not been applied in parallel to nondestructive measurements of Si/SiO_2.

The IPE, MPPE, and EFISH processes are illustrated in Fig. 2. MPPE is sensitive to the total potential barrier in Si *and* SiO_2, while EFISH measures the electric field integral in Si alone. The two techniques therefore provide related information although MPPE remains sensitive to oxygen pressures as low as ~ 1 μTorr. From our experiments we observe several novel effects including (i) localization of charge in the laser-irradiated region during O_2 exposure, (ii) irreversible electron transfer to SiO_2 traps after O_2 exposure, (iii) slow redistribution of trapped charge, and (iv) photoinduced electron trapping in the oxide film *in vacuo* with areal density as high as $\sim 10^{11}$ cm^{-2}.

The remainder of this paper is organized as follows. In the next section we outline the basic theoretical formalism for EFISH in Si/SiO_2 with emphasis on how charge transfer yields time-dependent SHG signals. We also briefly review concepts related to MPPE processes. Section III describes the experimental techniques, while Sec. IV presents results of the EFISH and MPPE experiments. The paper concludes with a summary of our major findings.

II. THEORETICAL CONSIDERATIONS

In anticipation of the experimental results that follow, we model the EFISH and MPPE response of Si/SiO_2 at 295 K illuminated by pulses from two laser systems. The first system (''Ti-osc'') is a Kerr-lens-mode-locked Ti:sapphire laser emitting a 76-MHz train of 130-fs pulses, tunable from 720 to 825 nm with average power up to 1 W. The second system (''Ti-amp'') uses the Ti-osc to seed a regenerative amplifier which provides 2-μJ, 150-fs, 800-nm pulses at repetition rate 250 kHz. The pulses illuminate a 100-μm^2 area producing peak irradiances up to 25 GW/cm^2. As Fig. 2 indicates, it is weak nonlinear absorption processes that lead to electron transfer to SiO_2 and so alter the extent of the space charge region in Si. However, much stronger linear optical absorption produces high electron-hole densities which screen the space-charge electric field. We now outline how EFISH and MPPE probe the charge distribution in Si/SiO_2.

A. Electric field-induced second-harmonic generation in Si/SiO_2

1. Sources for SHG

In the absence of electric fields, SHG in centrosymmetric media such as Si and amorphous SiO_2 is due to surface electric dipole and bulk quadrupole contributions.[18,39–41] The surface polarization density at the second-harmonic frequency is

$$P_{SD,i}^{(2\omega)} = \chi_{ijk}^{(2),S} E_j^{\omega} E_k^{\omega}, \tag{2.1}$$

while the bulk-quadrupole polarization can be written as

$$P_{BQ,i}^{(2\omega)} = \Gamma_{ijkl} E_j^{\omega} \nabla_k E_l^{\omega}. \tag{2.2}$$

Here, $\chi_{ijk}^{(2),S}$ is the surface dipole susceptibility tensor, Γ_{ijkl} the bulk quadrupole susceptibility tensor and E_j^{ω} the fundamental beam electric field. When a dc electric field is present there is also a bulk-dipole polarization density:

$$P_{BD,i}^{(2\omega)} = \chi_{ijkl}^{(3)} E_j^{\omega} E_k^{\omega} E_l^{\mathrm{dc}}, \tag{2.3}$$

where $\chi_{ijkl}^{(3)}$ is the EFISH susceptibility and E^{dc} the local dc electric field. Since $|\chi^{(3)}|$ is $\sim 10^4\times$ smaller in SiO_2 than in Si, EFISH from Si/SiO_2 is dominated by the near-interface electric field in Si. In MOS structures EFISH contributes[18,19,42] significantly to SHG for $E^{dc} \geqslant 10^5$ V/cm.

A more detailed model of the SHG response considers the electric-field distribution in Si including screening.[43] For Boltzmann statistics, and an excess electron-hole concentration N in Si, the Debye screening length is

$$\lambda_D = \left(\frac{\epsilon_{\mathrm{Si}} k_B T}{N e^2} \right)^{1/2}, \tag{2.4}$$

with static dielectric permittivity ϵ_{Si}, Boltzmann's constant k_B and electron-hole plasma temperature T. The time scale for screening is set by the plasma frequency:

$$\omega_p = \left(\frac{N e^2}{\epsilon_{\mathrm{Si}} m^*} \right)^{1/2}, \tag{2.5}$$

where the conductivity effective mass is $m^* = 0.26 m_e$.

The time dependence of the near-interface density of excess carriers in Si is shown schematically in Fig. 3 for both the Ti-amp and Ti-osc. We take a surface-recombination

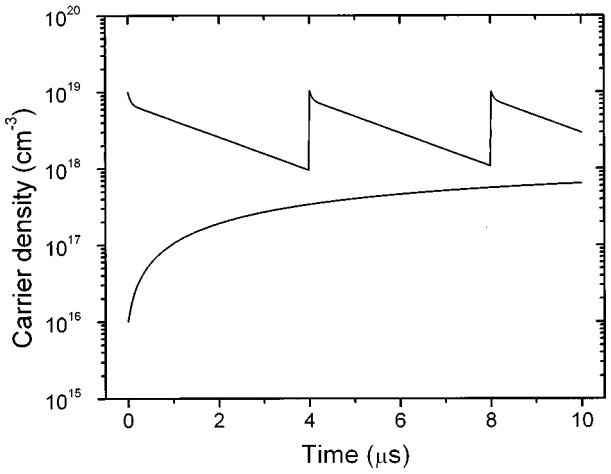

FIG. 3. Interface excess carrier density in Si due to $\hbar\omega = 1.55$ eV laser sources with average irradiance $= 0.6$ kW/cm^2. Upper curve, 250-kHz, 150-fs Ti-amp. Lower curve, 76-MHz, 130-fs unamplified Ti-osc.

velocity[44,45] $S \simeq 10^3$ cm s^{-1}, a bulk recombination time of 3 μs and an absorption coefficient[46] $\alpha(\omega) = 10^3$ cm^{-1} at $\lambda \approx 800$ nm. For the Ti-osc $N \sim 10^{18}$ cm^{-3}, $\lambda_D \sim 4$ nm at 295 K, and $\omega_p^{-1} \sim 30$ fs. Cumulative pulse-to-pulse effects determine N since the 13-ns interval between pulses is short relative to the time-scale for carrier recombination. For the Ti-amp a *peak* $N \sim 10^{19}$ cm^{-3} results, with $\lambda_D \sim 1$ nm and $\omega_p^{-1} \sim 10$ fs. The source region for EFISH in Si is limited by screening, and not by optical absorption: $\lambda_D < \alpha^{-1}(2\omega) \ll \alpha^{-1}(\omega)$ for[46] $\alpha^{-1}(2\omega) \sim 80$ nm.

The EFISH response is related to the integral of the screened electric field in Si, and thus to an areal density σ of negative charges on the oxide surface (Fig. 2). In what follows, the greatest contribution to σ is charge transfer from Si to SiO_2 due to multiphoton absorption in Si. Any interface or oxide trapped charge can also be incorporated into σ. From Gauss's law, the electric field in Si at the Si/SiO_2 interface is

$$E^{\rm dc}(z=0)\hat{\mathbf{z}} \equiv E^{\rm dc}_{int}\hat{\mathbf{z}} = \frac{e\sigma}{\epsilon_{Si}}\hat{\mathbf{z}}, \tag{2.6}$$

where $\hat{\mathbf{z}}$ is the outward normal to the surface. For $z<0$ in the semi-infinite substrate, the *net* charge density in the screened space-charge layer is

$$\delta N(z) = \delta N(0)\exp(z/\lambda_D). \tag{2.7}$$

Since the electric field vanishes as $z \to \pm\infty$,

$$\mathbf{E}^{\rm dc}(z) = \frac{\delta N(0) e \lambda_D}{\epsilon_{\rm Si}} \exp(z/\lambda_D)\hat{\mathbf{z}} \quad \text{with} \quad \int_{-\infty}^{0} \delta N(Z)\,dz = \delta N(0)\lambda_D = \sigma. \tag{2.8}$$

The electric-field integral over the SHG absorption depth is

$$\int_{-\alpha^{-1}(2\omega)}^{0} E^{\rm dc}(z)\,dz = \frac{e\sigma}{\epsilon_{\rm Si}}\lambda_D\{1-\exp[-\alpha^{-1}(2\omega)/\lambda_D]\} \approx \frac{e\sigma}{\epsilon_{\rm Si}}\lambda_D \quad \text{for } \lambda_D \ll \alpha^{-1}(2\omega). \tag{2.9}$$

The interface electric field $E^{\rm dc}_{int}$ and the surface charge density σ can be estimated by comparing the EFISH response to that in dc-biased MOS structures.

The effective SHG polarization density can now be written as

$$P^{(2\omega)}_{eff,i} = \epsilon_0 \chi^{(2),S}_{ijk} E^{\omega}_j E^{\omega}_k + \epsilon_0 \alpha^{-1}(2\omega)\Gamma_{ijlk} E^{\omega}_j \nabla_l E^{\omega}_k + e\epsilon_0 \frac{\sigma}{\epsilon_{\rm Si}} \lambda_D \chi^{(3)}_{ijkz} E^{\omega}_j E^{\omega}_k, \tag{2.10}$$

where the integration over the SHG absorption depth for the bulk quadrupole and EFISH contributions is implicit in the second and third terms, respectively. For fixed orientations of $E^{(\omega)}_k$ and $E^{(\omega)}_l$, the SHG intensity is

$$I^{(2\omega)} \propto \left|\chi^{(2),S}_{eff} + \Gamma_{eff}\alpha^{-1}(2\omega) + e\chi^{(3)}_{eff}\sigma\lambda_D/\epsilon_{\rm Si}\right|^2 [I^{(\omega)}]^2, \tag{2.11}$$

where $I^{(\omega)}$ is the fundamental intensity. The effective scalar susceptibilities imply a sum of tensor elements weighted by Fresnel factors.[40,47]

2. SHG time dependence

The time dependence of σ is given by

$$\frac{d\sigma}{dt} = \frac{(\sigma_0 - \sigma)}{\tau_g} - \frac{\sigma}{\tau_d}, \tag{2.12}$$

for a density σ_0 of empty charged sites at $t=0$, dissipation time τ_d, and accumulation time τ_g. Since $\sigma_\infty \to \sigma_0$ as $\tau_d \to \infty$, a dissipation process is required to attain a steady state with $\sigma_\infty < \sigma_0$. Possible dissipation processes include Coulomb repulsion among adsorbed O_2 molecules, carrier recombination, and exchange between the adsorbed and gas phases. As σ increases, the potential barrier to IPE and τ_g both increase. Neglecting tunneling,[48] the rate of n-photon IPE through SiO_2 of thickness d_{ox} is

$$\frac{1}{\tau_g(\sigma)} = \frac{1}{\tau_g(0)}\left[1 - \frac{e^2\sigma d_{ox}}{\epsilon_{\rm Si}(n\hbar\omega - \hbar\omega_T)}\right]^2 \propto \left(n\hbar\omega - \hbar\omega_T - \frac{e^2\sigma d_{ox}}{\epsilon_{\rm Si}}\right)^2. \tag{2.13}$$

The change in the IPE threshold $\hbar\omega_T$ due to surface charge σ is $eE^{\rm dc}_{int}d_{ox} = e^2\sigma d_{ox}/\epsilon_{\rm Si}$. The path length for electron energy loss may actually exceed d_{ox} due to the space-charge electric field in Si. The IPE energy dependence is due to Kane,[49,50] and will be described below in connection with MPPE. With 1.55 eV $\leqslant \hbar\omega \leqslant$ 1.72 eV and $\hbar\omega_T \approx 4.2$ eV, the lowest-order multiphoton absorption processes leading to IPE from the Si VB to the SiO_2 CB have $n=3$. IPE may be due to direct three-photon absorption, cascaded linear and two-photon absorption, or a combination thereof. For sufficiently large σ_0, the maximum σ corresponds to $\tau_g^{-1} = 0$ in

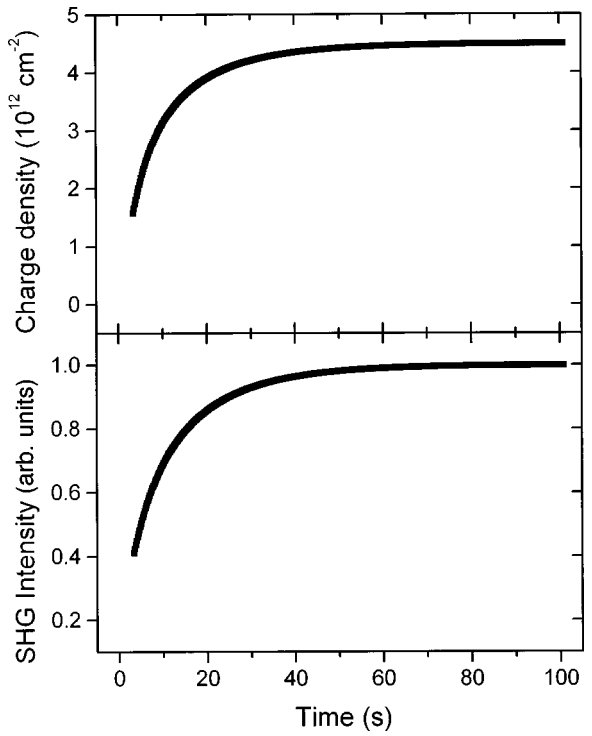

FIG. 4. (a) Surface charge density vs time. Points, IPE-surface-charging model with $\tau_g(0)=10$ s, $\tau_d=100$ s. (b) Corresponding SHG intensity vs time.

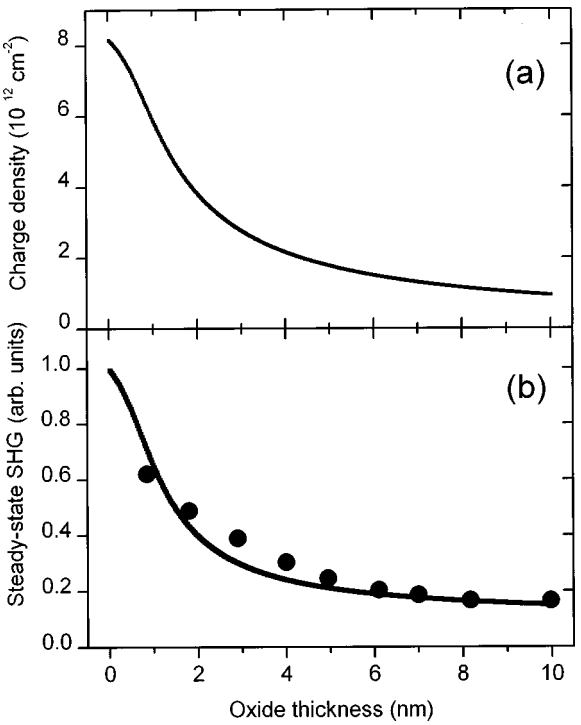

FIG. 5. (a) Steady-state surface charge density vs oxide thickness. IPE-surface-charging model with $\tau_g(0)=10$ s, $\tau_d=100$ s. (b) Steady-state SHG intensity. Line, numerical model. Circles, our data from Ref. 7.

Eq. (2.13), or $\sigma \leqslant 1.6\times 10^{13}$ cm^{-2} for three-photon IPE, with $\hbar\omega=1.55$ eV and $d_{ox}=1.6$ nm.

The numerical solution $\sigma(t)$ of Eqs. (2.12) and (2.13) and the SHG intensity are shown in Fig. 4 for three-photon IPE with $\sigma=0$ at $t=0$. In anticipation of typical experimental conditions, we have used $E_{int}^{\rm dc}=10^6$ V cm^{-1} or $\sigma_0=10^{13}$ cm^{-2}, and have taken the ratio of the steady-state EFISH contribution to field-independent terms in Eq. (2.11) to be 1.24. Phenomenological values[7] for Si/SiO_2 exposed to air were used for $\tau_g(0)$ and τ_d.

Equation (2.13) implies that greater electron-energy loss occurs in thicker oxides. IPE is totally suppressed when

$$d_{ox}=d_{ox,C}=\frac{(n\hbar\omega-\hbar\omega_T)\epsilon_{\rm Si}}{e^2\sigma_\infty}. \tag{2.14}$$

Assuming $\sigma_\infty=10^{13}$ cm^{-2}, $d_{ox,C}\sim 3$ nm. Figure 5 depicts the exact steady-state solution σ_∞ of Eqs. (2.12) and (2.13) for different d_{ox}. The corresponding SHG intensity is also shown. The same ratio between EFISH and field-independent SHG was used as in Fig. 4. A convenient analytical approximation is $\sigma_\infty=\sigma_{max}\exp(-d_{ox}/d_{ox,C})$. Both the calculation using Eq. (2.14) and the numerical solution in Fig. 5(b) agree with $d_{ox,C}\approx 3.5$ nm from the data of Ref. 7. The discrepancy for $d_{ox}<d_{ox,C}$ may exist because our model excludes scattering and restrictions on the electron momentum.

From scaling relations[51] for multiphoton absorption,

$$\frac{1}{\tau_g(0)}=\frac{K_n[I^{(\omega)}]^n l(1-R)^n R_L\tau_p}{n\hbar\omega\ \ \sigma_0}, \tag{2.15}$$

for n-photon absorption coefficient K_n in Si, reflectance R, and electron mean-free path[52] $l\simeq 10$ nm. Equation (2.15) is weighted by the duty cycle $R_L\tau_p$ of a pulsed laser with repetition rate R_L and pulse duration τ_p. For simplicity the charge-transfer efficiency is set to unity and the electron momentum is unrestricted. With $K_3\simeq 10^{-6}$ cm^3/(GW)^2, $R=0.2$, and $I^{(\omega)}=20$ GW/cm^2, we obtain $\tau_g(0)\sim 100$ s for the Ti-amp, in good agreement with observations presented here and in Ref. 7. The corresponding time-averaged IPE electron flux is 10^{11} cm^{-2} s^{-1}. For the Ti-osc the observed rise times are 0.1 to 10 s, depending on the photon energy and $I^{(\omega)}$. However, $n=3$ and $I^{(\omega)}=0.06$ GW/cm^2 in Eq. (2.15) give $\tau_g(0)\sim 10^7$ s for the less-intense Ti-osc source. Given the large carrier density excited by linear absorption ($N\sim 10^{18}$ cm^{-3}), cascaded two- and one-photon absorption may dominate IPE for the Ti-osc. Assuming $n=2$ and $K_2=10$ cm/GW (Ref. 53) in Eq. (2.15), and taking the efficiency of free carrier absorption to be $\sim 10^{-4}$ (corresponding to a conservative absorption cross section of $\sim 10^{-17}$ cm^{-2}) one finds $\tau_g(0)\sim 10^2$ s, much closer to the value observed experimentally.

3. SHG anisotropy and spectroscopy

A partial separation of the contributions to the anisotropic SHG response of Si/SiO_2 confirms that the time-dependent part of SHG is EFISH. As discussed in Refs. 18 and 40, in Si(100) the p-polarized SHG intensity due to a p-polarized fundamental is

$$I^{(2\omega)}\propto|a_0+a_4\cos(4\psi)|^2. \tag{2.16}$$

Here, ψ denotes sample rotation about the surface normal with $\psi=0$ for a [011] axis in the plane of incidence. The isotropic coefficient a_0 comprises interface-dipole, EFISH, and bulk-quadrupole contributions. Since the fourth-rank Γ_{ijlk} alone can produce a fourfold anisotropy, a_4 represents only bulk-quadrupole contributions. The signature of EFISH is increasing $|a_0|$ and decreasing $|a_4|/|a_0|$ for increasing E_{int}^{dc}.

A two-photon resonance of the bulk-allowed contribution[16,20,21] at $2\hbar\omega=3.4$ eV in both Si and Si/SiO_2 was first reported[13] by Daum *et al.* This SHG feature is redshifted relative to the nearby E_0' and E_1 resonances in the linear response of Si. Daum *et al.* attributed[13] the redshift to inhomogeneously strained near-interface Si layers. Studies of dc-biased MOS structures[20,21] exhibit a weak interface dipole peak at 3.25 eV and a strong EFISH peak near 3.4 eV. Both resonant features contribute only to a_0 in Eq. (2.16). For the purposes of identifying EFISH processes, the resonant enhancement of $|a_0|$ and decrease of $|a_4|/|a_0|$ with increasing E_{int}^{dc} are most pronounced near $2\hbar\omega=3.4$ eV.

B. Multiphoton photoemission

Photoemission is sensitive to changes in the energy ϕ needed to emit an electron from the medium.[54] In this paper, ϕ increases as the surface charge density increases. For MPPE from metals,[55,56] the current density **J** emitted from the sample is a sum of *n*-photon contributions $\mathbf{J}_n$ where

$$|\mathbf{J}_n|=\sigma_n[I^{(\omega)}]^n, \tag{2.17}$$

with the *n*-photon ionization cross section being

$$\sigma_n=a_n\left(\frac{e}{\hbar\omega}\right)^n A\ \ (1-R)^n T^2\ \ F\left(\frac{n\hbar\omega-\phi}{k_B T}\right). \tag{2.18}$$

Here, A is the Richardson coefficient ($120\ \mathrm{A\,cm^{-2}\,K^2}$), F the Fowler function, and T the electronic temperature. The constant of proportionality a_n is usually determined empirically,[57] with

$$a_n\propto\frac{p\ \ K_{n,PE}}{2\alpha(\omega)+1/l}, \tag{2.19}$$

where p is the electron escape probability and $K_{n,PE}$ the photoemissive part of K_n. The charge emitted is the integral of $\mathbf{J}\cdot\hat{\mathbf{z}}$ over the surface area and the pulse duration.

A model of MPPE in semiconductors replaces F in Eq. (2.18) with expressions due to Kane[49] which take least-order energy band expansions about ϕ for the electronic density of states. Also T may not be well-defined for nonequilibrium carriers generated during a 150-fs Ti-amp pulse, but a more detailed model for the transient-carrier distributions is not justified at this stage. The integrated photoelectric yield[49,58] is

$$Y_{PE}\propto\left(\frac{e}{\hbar\omega}\right)^n[n\hbar\omega-(\phi+\Delta\phi)]^m\ \ (I^{(\omega)})^n. \tag{2.20}$$

Here we use $\Delta\phi$ to represent changes in ϕ due to photo-induced charge transfer. The effective ϕ is determined by the initial state, which may be a VB state, mid-gap defect state,[59] or a CB state populated by linear absorption. Equation (2.20) can be modified[55,57] to reflect multiple initial states. For MPPE from the VB edge in Si, $\phi=\phi_{id}=5.15$ eV for indirect transitions, and $\phi=\phi_d=5.45$ eV for direct transitions.[58] Figure 2 depicts three-photon MPPE from the CB with $3\hbar\omega=4.65$ eV and $\phi_{3\hbar\omega}=\phi_d-E_{g,id}\approx 4.3$ eV, where $E_{g,id}$ is the minimum (indirect) band gap of Si. For four-photon MPPE, $4\hbar\omega=6.20$ eV and $\phi_{4\hbar\omega}=\phi_d$. The relative importance of three- and four-photon MPPE can be estimated from Wherret's scaling relations for multiphoton absorption.[51] The *n*-photon and $(n-1)$-photon absorption processes are related by $K_n(I^{(\omega)})^n/K_{n-1}(I^{(\omega)})^{n-1}=I^{(\omega)}/I_c$. Here, $I_c\sim 10^7$ GW/cm^2 is the critical irradiance at which $(n-1)$ photon absorption in Si matches *n*-photon absorption. In this paper, $I^{(\omega)}\leqslant 25$ GW/cm^2 and $I^{(\omega)}/I_c\sim 10^{-6}$. However, given the high-electron density excited to the CB by a single Ti-amp pulse ($N\sim 10^{19}$ cm^{-3}), the four-photon process is not likely to overwhelm the three-photon process on the basis of the density of initial states. Thus, the efficiency of sequential linear and three-photon MPPE processes may be higher than that of direct four-photon MPPE. One usually takes $m=2$ in Eq. (2.20) for direct MPPE dominated by bulk processes. For near-threshold ($[n\hbar\omega-\phi]<0.1$ eV) indirect photoemission,[49,50,58] $m=5/2$ is expected. We shall use $m=2$, since $3\hbar\omega-\phi_{3\hbar\omega}\sim 0.3$ eV. As Ref. 37 indicates, neither Coulomb forces nor three-body electron heating in the SiO_2 CB are expected to cause photoelectron energy shifts for $I^{(\omega)}\leqslant 25$ GW/cm^2.

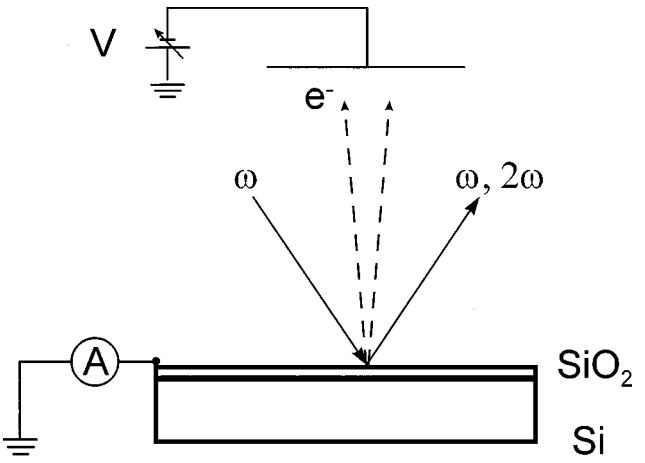

FIG. 6. Geometry used to measure SHG and MPPE: *V*-collector potential.

III. EXPERIMENT

The geometry for MPPE and SHG experiments is shown in Fig. 6. The Ti-amp and Ti-osc laser sources were described in Sec. II. Unless otherwise stated, samples were irradiated by 150-fs pulses from the Ti-amp source. For $I^{(\omega)}=25$ GW/cm^2 in a $100-\mu$m-diameter spot, time-averaged MPPE currents were $\leqslant 1$ nA (10^{14} electrons/cm^2 s). For measurements of MPPE alone, a normal incidence geometry could be used. For simultaneous MPPE and EFISH measurements, *p*-polarized laser radiation was incident at 45°. As shown in Fig. 7, a polarizer, Pellin-Broca prism, and filters selected the *p*-polarized component of the

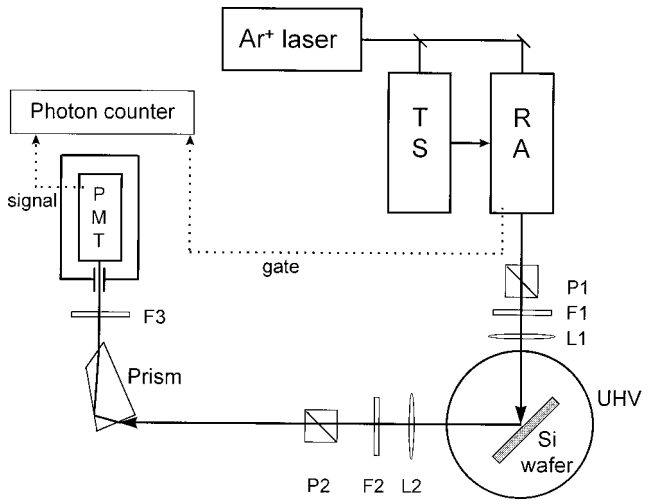

FIG. 7. Optical layout for SHG: TS, Ti:sapphire laser; RA, regenerative amplifier; P1,P2, cube polarizers. F1,F2,F3, filters; L1,L2 lenses; PMT, photomultiplier tube; UHV, ultrahigh vacuum chamber.

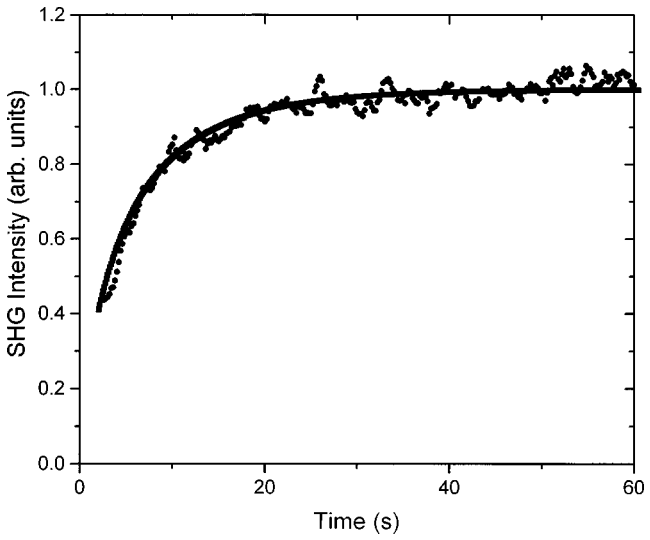

FIG. 8. Time-dependent SHG from Si/SiO_2 in air illuminated by *p*-polarized $\lambda = 800$ nm laser light. Scatter-plot, data. Curve, IPE-surface-charging model.

reflected SHG, which was detected by a photomultiplier tube (PMT). Gated by the Ti-amp *Q* switch, a photon counter recorded the SHG signal and subtracted a near-zero dark signal. Gated photon counting yields high sensitivity and high signal-to-noise measurements despite the low SHG conversion efficiency ($\sim 10^{-13}$).

The Ti-osc was used for spectroscopic SHG measurements with $1.55\ \text{eV} < \hbar\omega < 1.72\ \text{eV}$. The 200-mW-average-power, *p*-polarized beam impinged at a 45° angle of incidence on a Si/SiO_2 sample in air. The Ti-osc power was constant within 15% across the tuning range. The photon counter was gated by a 300-Hz mechanical chopper placed in the ω beam. To correct for the PMT spectral response and changes in peak irradiance with ω, the signal was normalized to the SHG from a quartz crystal reference. The apparatus was otherwise the same as in the Ti-amp experiments.

The sample chamber was maintained at pressures $< 1 \times 10^{-7}$ Torr prior to O_2 exposure. For measurements of charge trapping in vacuum, the chamber achieved a base pressure $< 10^{-9}$ Torr. A quadrupole mass spectrometer detected no significant amount of O_2 following gas exposures. Ultrahigh purity ($\geqslant 99.994\%$)O_2 was used.

A grounded picoammeter measured a positive current equal in magnitude to the MPPE current via a wire contact to the sample surface. A $\sim 1\ \text{cm}^2$ collector plate could be placed 1 cm from the sample. As the collector potential *V* increased to several volts with $V > 0$, the MPPE current increased fourfold, then reached a plateau when all photoelectrons were collected. Similar results were obtained for negative currents, $V = 0$, and a sample held at negative potential. Photo-induced changes in ϕ were confined to the area probed by the laser. Translating the sample by $> 100\ \mu\text{m}$ is effectively the same as using a virgin sample. The sample was also heated from time to time to remove the effects of previous exposures, but all MPPE/SHG experiments were conducted at 295 K.

The samples were polished *n*-type Si(100) wafers (resistivity $20-100\ \Omega\,\text{cm}$) $2\ \text{mm} \times 12\ \text{mm}$ in area and 0.3 mm thick. The existing SiO_2 film was grown in steam at 850 K and was determined by ellipsometry to be 1.6 nm thick. The essential features of experiments using other samples, including *n*-type Si(100) with device-quality dry oxides and *p*-type Si(100) anodically oxidized in HCl, are similar to those reported here; details will be reported elsewhere.[25]

IV. RESULTS AND DISCUSSION

Figure 8 presents a typical time-dependent *p*-polarized SHG trace for Si/SiO_2 in air exposed to $25\ \text{GW}\,\text{cm}^{-2}$ Ti-amp pulses. The increase in E^{DC} during laser exposure is well-described by the numerical solution of Eqs. (2.12) and (2.13). A fit to the data shown in Fig. 8 gives $\tau_g(0) = 6.7$ s and $\tau_d = 67$ s. To establish that the SHG enhancement is EFISH, we determined the spectral characteristics of the signal using Ti-osc as indicated in Fig. 9. The resonance in the isotropic (a_0) SHG component at $2\hbar\omega = 3.37$ eV ($\lambda = 735$ nm) is consistent with EFISH. Figure 10 shows the SHG anisotropy measured vs time at $\lambda = 735$ nm. Given the long recovery time τ_d, a distinct area of the sample was

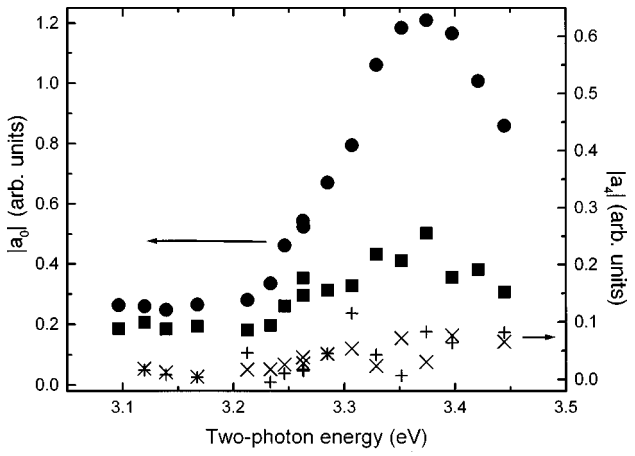

FIG. 9. SHG spectra of Si/SiO_2 in air. Left axis, initial (squares) and steady-state (circles) isotropic component $|a_0|$. Right axis, initial ($\times$) and steady-state ($+$) anisotropic component $|a_4|$.

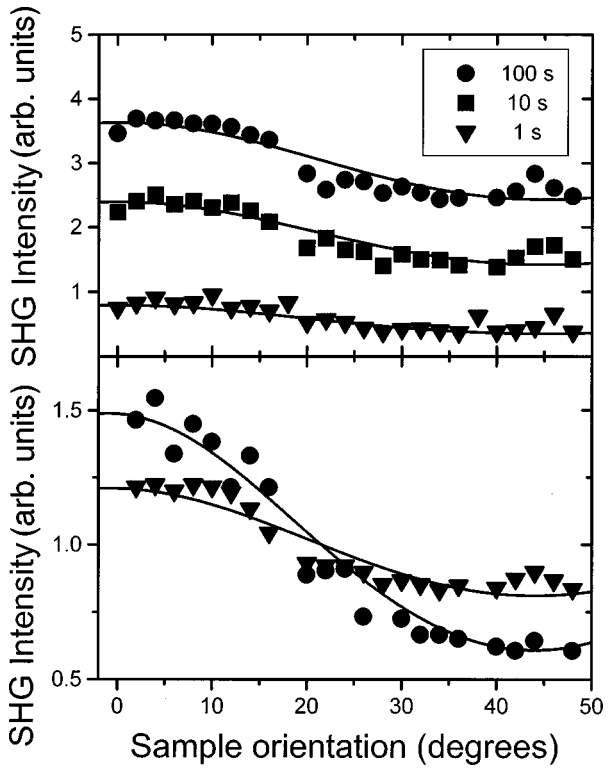

FIG. 10. SHG anisotropy on-resonance ($\hbar\omega = 1.69$ eV). Top, SHG response vs time. Bottom, initial (triangles) and steady-state (circles) SHG normalized to unity. Curves, fits to Eq. (2.16).

probed at each angle ψ. The upper figure indicates the anisotropy after 1, 10, and 100 s of laser exposure, corresponding to $|a_4|/|a_0| = 0.20$, 0.13 and 0.10, respectively. The lower figure presents the ''initial'' ($t = 0.33$ s) and ''steady state'' ($t = 290$ s) anisotropy, with $|a_4|/|a_0| = 0.22$ and 0.10, respectively. A comparison of these EFISH signatures with the data of Dadap *et al.* for MOS structures[20] indicates a field increase $\Delta E_{int}^{dc} \sim 3$ MV/cm.

We now consider MPPE from the same sample when illuminated in vacuum by Ti-amp pulses. Figure 11 shows a plot of MPPE current vs the peak irradiance. For constant collector potential V, the MPPE current obeys a power law

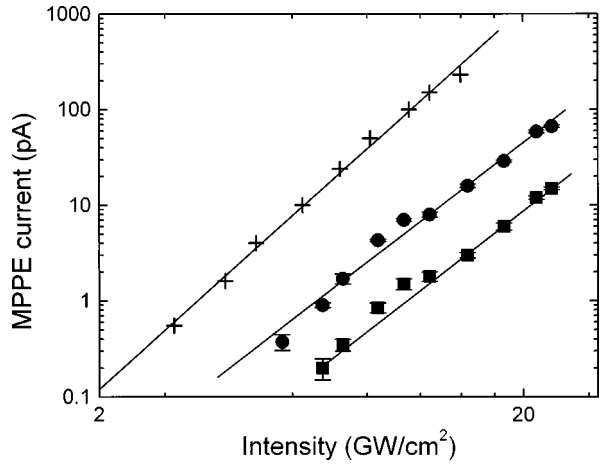

FIG. 11. MPPE vs peak irradiance. Lines, power laws with exponents n. Circles, collector bias $V = +60$ V, $n = 3.2$. Squares, $V = 0$, $n = 3.3$. Crosses, $n = 3.7$.

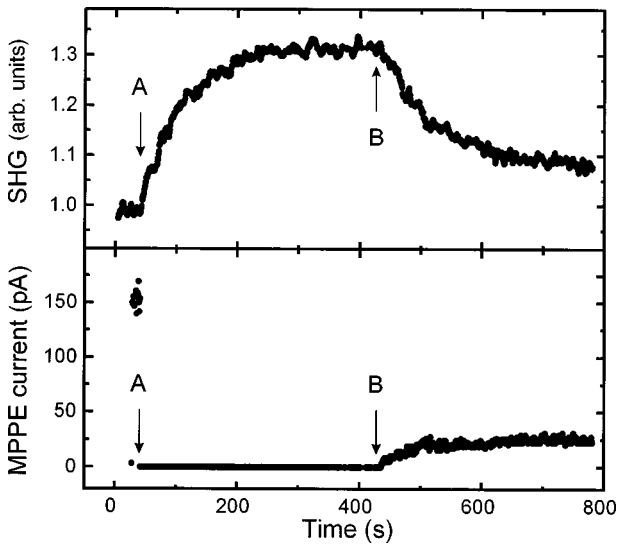

FIG. 12. SHG (top) and MPPE (bottom) during O_2 exposure: *A*, add 70 Torr O_2; *B*, pump to 10^{-7} Torr.

$Y_{PE} = k[I^{(\omega)}]^n$. The fitted $n = 3.3 \pm 0.1$, suggests that three-photon MPPE dominates.[59] However, $3\hbar\omega = 4.65$ eV, less than the VB-to-vacuum MPPE threshold ($\phi \sim 5.3$ eV). This suggests[37,59] MPPE from defect/ impurity states or CB states filled by linear absorption, with $\phi \sim 4.2$ eV. Note that the current-intensity curves with $V = 0$ and $V = +60$ V are parallel. This together with the absence of a plateau in the MPPE current at high $I^{(\omega)}$, even for $V = 0$, shows that MPPE is not limited by vacuum space charge effects. In what follows, all experiments used a grounded sample and collector.

Since the MPPE current could only be measured for $I^{(\omega)}$ over one order of magnitude, n cannot be determined to high precision. Figure 11 also shows data for a selected region of a sample, which yields very high MPPE currents, with $n \approx 3.7$. Variations in n across the sample surface suggest that ϕ is somewhat nonuniform. However, the *magnitude* of the MPPE current is similar even where n is obviously different. The average exponent for several similar measurements was $n = 3.7$. Thus, both three-photon and four-photon processes may contribute to the MPPE current. This exponent should not be overemphasized, however, since the actual irradiance-dependent distribution function probably cannot be described by a thermodynamic temperature, which Eq. (2.18) assumes. Intrinsic defects of the ultrathin oxide may also have some effect, but tunneling is not expected for an unbiased sample. Increased laser scattering and high MPPE currents were sometimes observed near the sample edges, suggesting mechanical damage. Such regions were easily excluded from study.

Figure 12 shows simultaneous SHG and MPPE measurements of photoinduced charging of the SiO_2 film during exposure to 70 Torr O_2 with $I^{(\omega)} = 20$ GW/cm^2. For this high-dose case, the relative change in the SHG intensity was $I^{(2\omega)}/I_0^{(2\omega)} = 1.3$. We estimate $E_{int}^{dc} \approx 1.5$ MV/cm from EFISH in MOS structures,[19] or $\sigma = 1 \times 10^{13}$ cm^{-2}. Suppression of MPPE due to charge accumulation is evident in the data of Fig. 12, bottom. Note that electron scattering from O_2 gas phase molecules has a negligible effect on MPPE. In the range from 1 to 1000 eV, the total electron scattering cross

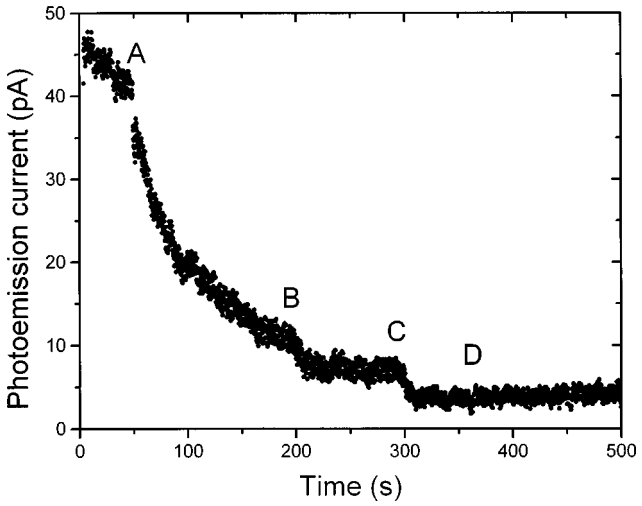

FIG. 13. MPPE response as $P(O_2)$ increases from 10 μTorr to *A*, 100 μTorr, *B*, 200 μTorr, *C*, 600 μTorr. *D*, evacuate chamber.

section[60] in O_2 is $\leqslant 10^{-15}$ cm^2. Only 0.01% of the MPPE flux is scattered from O_2 molecules at $P(O_2)=1$ atm.

As depicted in Fig. 12, the SHG and MPPE signals recover partially when the analysis chamber is evacuated. For $t>700$ s, $I^{(2\omega)}/I_0^{(2\omega)}=1.05$, $E_{int}^{dc}\approx 0.2$ MV/cm, and $\sigma\approx 1\times 10^{12}$ cm^{-2}. The changes in MPPE and SHG depend strongly on the gas used, with the strongest effects due to O_2.[7] MPPE and SHG maintain constant residual levels even when the laser beam is blocked for 5–10 min. This rules out artifacts due to sample heating. We therefore attribute the residual change to charge transfer to SiO_2 traps, possibly from adsorbed superoxide (O_2^-) anions[31] formed by IPE from Si.

Figure 13 shows the MPPE response at $I^{(\omega)}=25$ GW/cm^2 for $10^{-5}<P(O_2)<10^{-3}$ Torr. While significant O_2-stimulated SHG is observed only for $P(O_2)\geqslant 1$ Torr, MPPE extends observations to $P(O_2)\sim 10^{-5}$ Torr. The gradual decline in MPPE current represents O_2-assisted, IPE-induced charge accumulation on the SiO_2 film. The reduction of the MPPE current upon evacuation of the chamber remained evident following a 10-min interval during which the laser beam was blocked.

Figure 14 illustrates a peculiar MPPE response of particular ''virgin'' areas of a sample in vacuum exposed to the Ti-amp at $I^{(\omega)}=25$ GW/cm^2. We attribute the decrease of the MPPE current to direct, i.e., gas-independent, SiO_2 trapping processes. The effect remains at least for several hours. Since there is no corresponding increase in SHG, the trapped charge density here is $\sim 5\times 10^{11}$ cm^{-2} or less from comparison to the data of Fig. 12. While the residual drop in MPPE due to O_2 exposure is evident anywhere on the sample, direct trapping normally has a lesser influence because it is confined to specific areas.

The high sensitivity of MPPE can be exploited to measure charge redistribution from the sample area irradiated by a normal-incidence Ti-amp beam, as shown in Fig. 15. The threshold shift $\Delta\phi$ was calculated using Eq. (2.20). With $P(O_2)=30$ Torr, a 100-μm-diameter region was irradiated for several minutes. When the chamber was evacuated, the

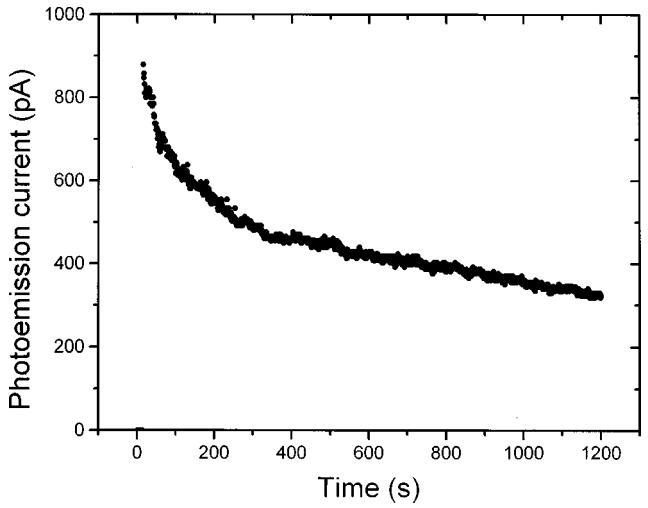

FIG. 14. Site-specific decrease of MPPE in vacuum.

MPPE current remained reduced, as in Figs. 12 and 13. The Ti-amp beam was blocked and then briefly unblocked at 5-min intervals so that the MPPE current could be recorded. The circles in Fig. 15 indicate the gradual decrease in ϕ (increase in Y_{PE}) in the irradiated region. A similar experiment was conducted in which the sample was translated 150 μm perpendicular to the Ti-amp beam following the initial irradiation and O_2 exposure. The second MPPE measurement indicates a slow increase in ϕ (decrease in Y_{PE}), depicted by the squares in Fig. 15. The slow decrease (increase) in ϕ inside (outside) the treated area indicates lateral migration of charge in the oxide film. Both of the above experiments would give similar results if laser-induced heating were relevant. We estimate an effective diffusion constant $D\sim 10^{-7}$ cm^2/s for the trapped charge. The charge transport may be driven by Coulomb repulsion, not thermally activated. Since trap states lie in the band gap of the insulating SiO_2, transport may be limited to trap-to-trap hopping. Measurements of O_2 desorption using a mass spectrometer did not detect any change in $P(O_2)$ at the 10^{-12} Torr level

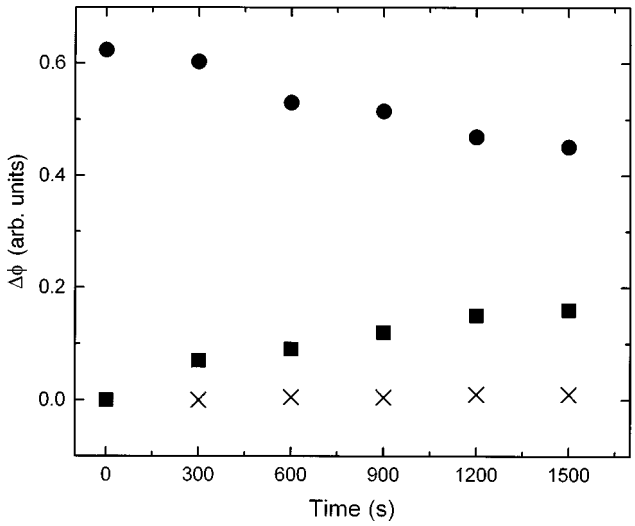

FIG. 15. MPPE threshold shift inside (circles) and outside (squares) the laser-irradiated region after 30 Torr O_2 exposure. Crosses, control measurement on an untreated sample.

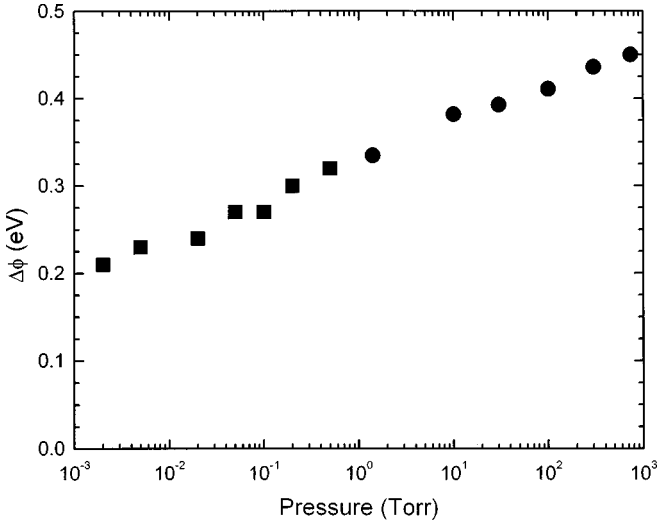

FIG. 16. Steady-state threshold shift measured by MPPE (squares) and SHG (circles) during O_2 exposure.

within 5 min of evacuation of the analysis chamber. Therefore, redistribution of charge is not related to O_2.

The sample was then heated to 700 K for 20 s to detrap electrons in SiO_2, then cooled to 295 K. As a control, a MPPE measurement was conducted in vacuum, but without prior O_2 exposure. As indicated by the crosses in Fig. 15, ϕ was almost constant. The very small increase in ϕ may represent direct trap filling. Furthermore, no lateral charge redistribution was measured in a region of the sample exhibiting direct trapping in vacuum similar to that represented in Fig. 14. This indicates that the O_2-assisted and *in vacuo* trapping mechanisms involve distinct trap sites.

Figure 16 compares MPPE and EFISH $\Delta\phi$ data over a broad range of $P(O_2)$. Each O_2 exposure lasted 200 s. SHG data were analyzed using Eq. (2.11). The maximum, $\Delta\phi \approx 0.45$ eV, exceeds the nominal 0.40 eV limit for IPE with $\hbar\omega_T = 4.25$ eV (Refs. 26 and 27) and $3\hbar\omega = 4.65$ eV. This may be because the reference EFISH data[19] refer to *p*-type MOS structures with $d_{ox} \geqslant 18$ nm. Nevertheless, we intend only to show how $\Delta\phi$ scales with $P(O_2)$, not to precisely calibrate EFISH. For three-photon MPPE, $\Delta\phi$ was calculated using Eq. 2.20 with $\phi = \phi_{3\hbar\omega} = 4.33$ eV.[58,61] The linear variation of $\Delta\phi$ with $\ln P(O_2)$ is consistent with Fowler-Guggenheim adsorption.[62] For repulsive interactions with interaction energy $u \geqslant 2k_BT$ between adatoms, the surface coverage is linear in $\ln P$ over several decades. At 1 Torr $\sigma \sim 10^{12}$ cm^{-2}, so $u \sim 6k_BT$ for singly charged adsorbates. The Coulomb forces implicit in the data of Fig. 16 should lead to redistribution of charge.

EFISH and MPPE are complementary techniques for measuring related charge-transfer phenomena in $Si/SiO_2/O_2$ in different regimes of O_2 pressure. EFISH is best suited to pressures $P(O_2) \geqslant 1$ Torr, where $\sigma \sim 10^{12}$ cm^{-2}, $E_{int}^{dc} \sim 10^6$ V/cm, and $\Delta\phi \geqslant 0.1$ eV. The more-sensitive MPPE can resolve $\Delta\phi \sim 0.01$ eV for $P(O_2) \sim 10^{-5}$ Torr, equivalent to $\sigma \sim 10^{11}$ cm^{-2}. However, for $P(O_2) \geqslant 1$ Torr, MPPE is totally suppressed and is limited to *in vacuo* measurements of residual effects. A biased collector anode might extend the sensitivity of MPPE to lower pressures.

V. CONCLUSIONS

We have shown that EFISH and MPPE methods can be combined to sensitively measure important charge trapping processes in/on ultrathin SiO_2 films on Si. Using both EFISH and MPPE, we observed O_2-assisted charging due to internal photoemission of electrons from the Si valence band to the SiO_2 conduction band, at surface negative charge densities up to 10^{13} cm^{-2}. The threshold changes $\Delta\phi$ in MPPE and electric field E^{dc} in EFISH were compared as an approximate cross-calibration of the two techniques. Residual charge transfer to SiO_2 traps is observed via EFISH and MPPE when O_2 gas is removed. MPPE measures the slow lateral redistribution of trapped charge, giving an effective diffusion constant $D \approx 10^{-7}$ cm^2/s at 295 K. In vacuum, the MPPE probe is also able to detect $\sim 10^{11}$ cm^{-2} electrons trapped in specific areas of the SiO_2 film. The relative sensitivity of EFISH and MPPE may differ in other regimes of photon energy/irradiance, or in materials with different third-order susceptibilities and multiphoton absorption mechanisms.

ACKNOWLEDGMENTS

We acknowledge stimulating discussions with Dr. J. Bloch and Dr. Z. Burshtein. We also thank Dr. J. Bardwell of the Institute for Microstructural Sciences for ellipsometry measurements. This research was funded by Photonics Research Ontario and the Natural Sciences and Engineering Research Council of Canada. H.M.vD. gratefully acknowledges the support of the Canada Council. J.G.M. received assistance from the Ontario Graduate Scholarship Program.

*Present address: DALSA, Inc., 605 McMurray Rd., Waterloo, Canada, ON N2V 2E9.

†Permanent address: Nuclear Research Center-Negev, P.O. Box 9001, Beer-Sheva, Israel.

‡Author to whom correspondence should be addressed. Electronic address: vandriel@physics.utoronto.ca

[1] E. Takeda, C. Y. Yang, and A. M. Hamada, *Hot-Carrier Effects in MOS Devices* (Academic, San Diego, 1995).

[2] E. M. Allegretto and J. A. Bardwell, J. Vac. Sci. Technol. A **14**, 2437 (1996).

[3] C. Svensson, in *The Si-SiO$_2$ System*, edited by P. Balk, Materials Science Monographs, Vol. 32 (Elsevier, Amsterdam, 1988), Chap. 5.

[4] P. Balk, in *The Si-SiO$_2$ System*, (Ref. 3), Chap. 1.

[5] D. J. DiMaria, E. Cartier, and D. Arnold, J. Appl. Phys. **73**, 3367 (1993).

[6] N. Shamir, J. G. Mihaychuk, and H. M. van Driel, J. Vac. Sci. Technol. A **15**, 2081 (1997).

[7] J. Bloch, J. G. Mihaychuk, and H. M. van Driel, Phys. Rev. Lett. **77**, 920 (1996).

[8] J. G. Mihaychuk, J. Bloch, Y. Liu, and H. M. van Driel, Opt. Lett. **20**, 2063 (1995).

[9] M. Cernusca, R. Heer, and G. A. Reider, Appl. Phys. B: Lasers Opt. **66**, 367 (1998).

[10] G. Lüpke, D. J. Bottomley, and H. M. van Driel, Phys. Rev. B **47**, 10 389 (1993).

[11] O. A. Aktsipetrov, A. A. Fedyanin, E. D. Mishina, A. A. Nikulin, A. N. Rubtsov, C. W. van Hasselt, M. A. C. Devillers, and T. Rasing, Phys. Rev. Lett. **78**, 46 (1997).
[12] J. I. Dadap, X. F. Hu, N. M. Russell, J. G. Ekerdt, J. K. Lowell, and M. C. Downer, IEEE J. Sel. Top. Quantum Electron. **1**, 1145 (1995).
[13] W. L. Daum, H.-J. Krause, U. Reichel, and H. Ibach, Phys. Rev. Lett. **71**, 1234 (1993).
[14] U. Emmerichs, C. Meyer, H. J. Bakker, H. Kurz, C. H. Bjorkman, C. E. Shearon, Jr., Y. Ma, T. Yasuda, Z. Jing, G. Lucovsky, and J. L. Whitten, Phys. Rev. B **50**, 5506 (1994).
[15] G. Lüpke, C. Meyer, U. Emmerichs, F. Wolter, and H. Kurz, Phys. Rev. B **50**, 17 292 (1994).
[16] C. Meyer, G. Lüpke, U. Emmerichs, F. Wolter, H. Kurz, C. H. Bjorkman, and G. Lucovsky, Phys. Rev. Lett. **74**, 3001 (1995).
[17] C. W. van Hasselt, M. A. C. Devillers, T. Rasing, and O. A. Aktsipetrov, J. Opt. Soc. Am. B **12**, 33 (1995).
[18] O. A. Aktsipetrov, A. A. Fedyanin, and M. C. Downer, in *Notions and Perspectives in Nonlinear Optics*, edited by O. Keller, Series in Nonlinear Optics, Vol. 3 (World Scientific, Singapore, 1996), pp. 301–339.
[19] O. A. Aktsipetrov, A. A. Fedyanin, E. D. Mishina, A. N. Rubtsov, C. W. van Hasselt, M. A. C. Devillers, and T. Rasing, Phys. Rev. B **54**, 1825 (1996).
[20] J. I. Dadap, X. F. Hu, M. H. Anderson, M. C. Downer, J. K. Lowell, and O. A. Aktsipetrov, Phys. Rev. B **53**, R7607 (1996).
[21] P. Godefroy, W. de Jong, C. W. van Hasselt, M. A. C. Devillers, and T. Rasing, Appl. Phys. Lett. **68**, 1981 (1996).
[22] C. Ohlhoff, G. Lüpke, C. Meyer, and H. Kurz, Phys. Rev. B **55**, 4596 (1997).
[23] C. Ohlhoff, C. Meyer, G. Lüpke, T. Löffler, T. Pfeifer, H. G. Roskos, and H. Kurz, Appl. Phys. Lett. **68**, 1699 (1996).
[24] A. Nahata, T. F. Heinz, and J. A. Misewich, Appl. Phys. Lett. **69**, 746 (1996).
[25] N. Shamir, J. G. Mihaychuk, H. M. van Driel, and H. J. Kreuzer (unpublished).
[26] R. Williams, Phys. Rev. **140**, A569 (1965).
[27] P. V. Dressendorfer and R. C. Barker, Appl. Phys. Lett. **36**, 933 (1980).
[28] G. Herzberg, *Spectra of Diatomic Molecules*, Molecular Spectra and Molecular Structure, Vol. 1 (Van Nostrand, New York, 1950), p. 459.
[29] G. J. Schulz, Rev. Mod. Phys. **45**, 423 (1973).
[30] P. J. Caplan and E. H. Poindexter, J. Appl. Phys. **52**, 522 (1981).
[31] P. J. Caplan, E. H. Poindexter, and S. R. Morrison, J. Appl. Phys. **53**, 541 (1982).
[32] J. R. Goldman and J. A. Prybyla, Phys. Rev. Lett. **72**, 1364 (1994).
[33] N. J. Halas and J. Bokor, Phys. Rev. Lett. **62**, 1679 (1989).
[34] J. Bokor and N. J. Halas, IEEE J. Quantum Electron. **25**, 2550 (1989).
[35] J. Bokor, Science **246**, 1130 (1989).
[36] P. Daguzan, S. Guizard, P. Martin, G. Petite, A. D. Santos, and A. Antonetti, J. Opt. Soc. Am. B **13**, 138 (1996).
[37] P. Daguzan, S. Guizard, K. Krastev, P. Martin, G. Petite, A. D. Santos, and A. Antonetti, Phys. Rev. Lett. **73**, 2352 (1994).
[38] J. Bokor, A. M. Johnson, R. H. Storz, and W. M. Simpson, Appl. Phys. Lett. **49**, 226 (1986).
[39] H. W. K. Tom, X. D. Zhu, Y. R. Shen, and G. A. Somorjai, Surf. Sci. **167**, 167 (1986).
[40] J. E. Sipe, D. J. Moss, and H. M. van Driel, Phys. Rev. B **35**, 1129 (1987).
[41] T. F. Heinz, in *Nonlinear Surface Electromagnetic Phenomena*, edited by H.-E. Ponath and G. I. Stegeman, Modern Problems in Condensed Matter Sciences, Vol. 29 (Elsevier Science, Amsterdam, 1991), Chap. 5.
[42] O. A. Aktsipetrov, A. A. Fedyanin, V. N. Golovinka, and T. V. Murzina, Opt. Lett. **19**, 1450 (1994).
[43] J. I. Dadap, P. T. Wilson, M. H. Anderson, M. C. Downer, and M. ter Beek, Opt. Lett. **22**, 901 (1997).
[44] E. Gaubas, A. Kaniava, and J. Vaitkus, Semicond. Sci. Technol. **12**, 1 (1997).
[45] S. K. Pang and A. Rohatgi, Appl. Phys. Lett. **59**, 195 (1991).
[46] D. F. Edwards, in *Handbook of Optical Constants of Solids*, edited by E. D. Palik (Academic Press, Orlando, 1985), pp. 547–569.
[47] D. J. Bottomley, G. Lüpke, J. G. Mihaychuk, and H. M. van Driel, J. Appl. Phys. **74**, 6072 (1993).
[48] Z. Burshtein and J. Levinson, Phys. Rev. B **12**, 3453 (1975).
[49] E. O. Kane, Phys. Rev. **127**, 131 (1962).
[50] G. W. Gobeli and F. G. Allen, Phys. Rev. **127**, 141 (1962).
[51] B. S. Wherret, J. Opt. Soc. Am. B **1**, 67 (1984).
[52] A. Zangwill, *Physics at Surfaces* (Cambridge University Press, Cambridge, 1988), Chap. 1.
[53] D. H. Reitze, T. R. Zhang, W. M. Wood, and M. C. Downer, J. Opt. Soc. Am. B **7**, 84 (1990).
[54] M. Cardona and L. Ley, in *Photoemission in Solids*, edited by M. Cardona and L. Ley, Topics in Applied Physics, Vol. 26 (Springer-Verlag, Berlin, 1978), Chap. 1.
[55] J. P. Girardeau-Montaut and C. Girardeau-Montaut, Phys. Rev. B **51**, 13 560 (1995).
[56] J. H. Bechtel, W. L. Smith, and N. Bloembergen, Phys. Rev. B **15**, 4557 (1977).
[57] R. Yen, J. Liu, and N. Bloembergen, Opt. Commun. **35**, 277 (1980).
[58] C. Sebenne, D. Bolmont, G. Guichar, and M. Balkanski, Phys. Rev. B **12**, 3280 (1975).
[59] W. J. Siekhaus, J. H. Kinney, D. Milam, and L. L. Chase, Appl. Phys. A: Solids Surf. **39**, 163 (1986).
[60] Y. Itikawa, in *Advances in Atomic, Molecular, and Optical Physics*, edited by M. Inokuti (Academic, San Diego, 1994), Vol. 33, pp. 253–274.
[61] *Semiconductors—Basic Data*, edited by O. Madelung (Springer-Verlag, Berlin, 1996).
[62] J. Oudar, *Physics and Chemistry of Surfaces* (Blackie & Son, Glasgow, 1975), Chap. 4.